



Proximity labeling of endogenous RICTOR identifies mTOR complex 2 regulation by ADP ribosylation factor ARF1

Received for publication, December 15, 2021, and in revised form, July 22, 2022. Published, Papers in Press, August 13, 2022.
<https://doi.org/10.1016/j.jbc.2022.102379>

Amelia K. Luciano¹, Ekaterina D. Korobkina¹, Scott P. Lyons², John A. Haley¹, Shelagh M. Fluharty¹, Su Myung Jung¹, Arminja N. Kettenbach^{2,3} , and David A. Guertin^{1,4,*}

From the ¹Program in Molecular Medicine, University of Massachusetts Chan Medical School, Worcester, Massachusetts, USA; ²Department of Biochemistry and Cell Biology, and ³Norris Cotton Cancer Center, Geisel School of Medicine at Dartmouth, Hanover, New Hampshire, USA; ⁴Department of Molecular, Cell and Cancer Biology, University of Massachusetts Chan Medical School, Worcester, Massachusetts, USA

Edited by Phyllis Hanson

Mechanistic target of rapamycin (mTOR) complex 2 (mTORC2) regulates metabolism, cell proliferation, and cell survival. mTORC2 activity is stimulated by growth factors, and it phosphorylates the hydrophobic motif site of the AGC kinases AKT, SGK, and PKC. However, the proteins that interact with mTORC2 to control its activity and localization remain poorly defined. To identify mTORC2-interacting proteins in living cells, we tagged endogenous RICTOR, an essential mTORC2 subunit, with the modified BirA biotin ligase BioID2 and performed live-cell proximity labeling. We identified 215 RICTOR-proximal proteins, including proteins with known mTORC2 pathway interactions, and 135 proteins (63%) not previously linked to mTORC2 signaling, including nuclear and cytoplasmic proteins. Our imaging and cell fractionation experiments suggest nearly 30% of RICTOR is in the nucleus, hinting at potential nuclear functions. We also identified 29 interactors containing RICTOR-dependent, insulin-stimulated phosphorylation sites, thus providing insight into mTORC2-dependent insulin signaling dynamics. Finally, we identify the endogenous ADP ribosylation factor 1 (ARF1) GTPase as an mTORC2-interacting protein. Through gain-of-function and loss-of-function studies, we provide functional evidence that ARF1 may negatively regulate mTORC2. In summary, we present a new method of studying endogenous mTORC2, a resource of RICTOR/mTORC2 protein interactions in living cells, and a potential mechanism of mTORC2 regulation by the ARF1 GTPase.

The mTOR kinase senses nutrient availability and growth factors to control cell metabolism, growth, proliferation, and survival. Its functions are split between two multisubunit protein complexes called mTOR complex 1 (mTORC1) and mTORC2. While mTORC1 regulation has been extensively defined (1, 2), primarily at the lysosome, a consensus model of mTORC2 regulation and localization has yet to emerge. A comprehensive list of functional mTORC2-interacting proteins remains elusive due in part to a knowledge gap regarding

proteins that interact with the complex. mTORC2 phosphorylates specific AGC family kinases including AKT, stress-induced serum and glucocorticoid kinase (SGK), and protein kinase C (PKC) α (3–5), but whether additional biologically relevant mTORC2 substrates exist is also unclear. Traditional protein–protein interaction studies often rely on overexpressed proteins and/or harsh purification conditions in which weak or transient protein interactions do not survive (6). To overcome this challenge, we developed a proximity labeling strategy to identify endogenous mTORC2-interacting proteins in live cells.

Proximity labeling is a powerful alternative to affinity purification/mass spectrometry (MS) based strategies because it provides higher sensitivity and biological relevance by utilizing an enzymatic reaction to mark interacting proteins within living cells (6). BioID2-based proximity labeling (6–8) utilizes a modified BirA biotin ligase from *Escherichia coli*, which is fused to a protein of interest and expressed in living cells. The promiscuous BioID2 enzyme converts inert biotin that is supplemented into the culture medium into highly reactive and short-lived biotinoyl-5'-adenosine monophosphate, which covalently attaches to lysine residues on proximal proteins within a 10 nm radius (6). The amount of labeling correlates with how long a protein is in proximity, negatively correlates with its distance from the enzyme, and ends at membrane boundaries. Biotinylated proteins are captured on a streptavidin affinity matrix and identified by MS. Proximity labeling has successfully mapped protein interaction networks associated with signal transduction pathways (e.g., MAPK (9), Hippo (10), Ras (11, 12), Hedgehog (13), adrenergic (14), and GPCR (15) signaling), organelles (16), and subcellular compartments (17).

mTORC2 includes the mTOR kinase, RICTOR, SIN1/MAPKAP1, and mLST8 subunits. In the absence of mLST8, RICTOR and SIN1 remain bound but no longer interact with mTOR. Here, we engineered cells to express BioID2 fused onto the amino terminus of endogenous RICTOR and confirmed that it forms functional mTORC2 complexes. Subsequent proximity labeling in the presence or absence of mLST8 identified 215 BioID2-RICTOR interacting proteins stratified as high, medium, and fair confidence interactors and

* For correspondence: David A. Guertin, David.Guertin@umassmed.edu.

Endogenous RICTOR/mTORC2 proximity labeling

either mTORC2 dependent (mLST8 present) or mTORC2 independent (mLST8 deleted). These included SIN1 and BioID2-RICTOR itself, as well as 80 proteins with previous links to mTORC2 and/or AKT signaling, validating the strategy. Unexpectedly, many BioID2-RICTOR interacting proteins are predominantly nuclear. We confirmed the presence of mTORC2 subunits in the nucleus suggesting an undefined nuclear function. Finally, we identified ARF GTPases and their regulators as mTORC2 proximal proteins. Functional studies support a model in which GTP-bound ARF1 associates with mTORC2 to inhibit AKT phosphorylation.

Results

Endogenous BioID2-RICTOR forms functional mTORC2 complexes

CRISPR/Cas9 engineering was used to insert a 3xFlag-BioID2 sequence upstream of exon 1 at the endogenous *RICTOR* loci generating an ~232 kDa BioID2-RICTOR fusion protein (Fig. S1, A and B, and Experimental procedures). Two independent BioID2-RICTOR HEK293E clonal cell lines were

generated in which homozygously tagged BioID2-RICTOR is distinguishable from control (untagged RICTOR) by its ~32 kDa band shift (Fig. S1B). To serve as a control for mTORC2 complex formation, we also generated BioID2-RICTOR clonal lines deleted for *MLST8* (BioID2-RICTOR^{mLST8Δ} cells), which encodes an mTOR-binding WD repeat protein required for mTORC2 assembly but not mTORC1 assembly (18–20) (Fig. S1C).

To gauge whether BioID2-RICTOR forms functional mTORC2 complexes, several key complex formation and signaling experiments were performed. Complex integrity was determined by coimmunoprecipitation (co-IP) of endogenous proteins. Endogenous mTOR co-IPs with RICTOR, SIN1 (mTORC2 subunit), mLST8 (mTORC1 & mTORC2), and RAPTOR (mTORC1) to a similar extent in control and BioID2-RICTOR cells, the latter indicated by blotting for both RICTOR or the Flag epitope (Fig. 1A). As expected, the mTOR interaction with BioID2-RICTOR and SIN1, but not RAPTOR, is lost in BioID2-RICTOR^{mLST8Δ} cells (Fig. 1A). Reciprocal co-IPs of endogenous RICTOR with either RICTOR or Flag antibodies confirm endogenous BioID2-RICTOR binds with

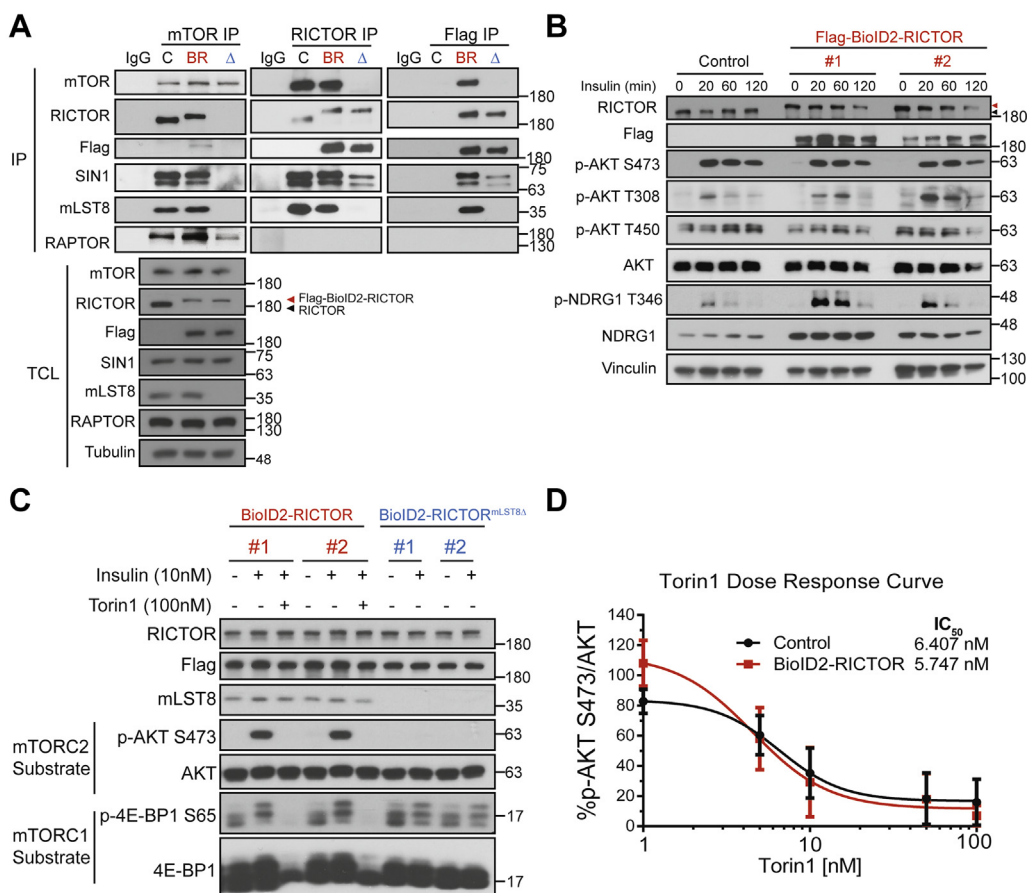


Figure 1. Flag-BioID2-RICTOR HEK293E cells have functional mTORC2 complexes. A, Western Blots of mTOR, RICTOR, and Flag immunoprecipitation from control (C, black), Flag-BioID2-RICTOR (BR, red), and Flag-BioID2-RICTOR^{mLST8Δ} (Δ, blue) demonstrating mTORC2 complex formation with RICTOR and Flag-BioID2-RICTOR only in the presence of mLST8. Red arrows point to Flag-BioID2-RICTOR; black arrows point to WT RICTOR. B, insulin stimulation (10 nM) time course in control and two Flag-BioID2-RICTOR clonal cell lines. Cells were put in serum-free DMEM for 5 h before stimulation. N = 3. C, insulin stimulation in each of the two clones of Flag-BioID2-RICTOR and Flag-BioID2-RICTOR^{mLST8Δ} cell lines. Cells were starved for 5 h and then insulin or insulin and mTOR inhibitor Torin1 were added. N = 3. D, torin dose response curve based on densitometry of p-AKT S473/total AKT in control and Flag-BioID2-RICTOR cells. Points are plotted as mean ± SEM. N = 3 for each experiment.

mTOR only in the presence of mLST8 (Fig. 1A). Moreover, RICTOR and SIN1 interact independently of mLST8, also consistent with previous reports (18). Notably, recent cryo-EM studies suggest the RICTOR N terminus projects away from the complex (21, 22) consistent with its ability to accept the N-terminal BioID2 tag without disrupting complex integrity.

Phosphorylation of AKT and NDRG1 (an SGK substrate) were examined to assess BioID2-RICTOR/mTORC2 function. Insulin time course experiments (10 nM) indicate similar insulin-stimulated kinetics of AKT S473 and NDRG1 T346 phosphorylation between control and clonal knock-in cells (Fig. 1B). AKT T308 phosphorylation is also induced with similar kinetics, while AKT T450 phosphorylation, a constitutive, cotranslational mTORC2-dependent phosphorylation site is stable in the knock-in cells (Fig. 1B). Moreover, insulin stimulated AKT S473 phosphorylation but not 4E-BP1 S65 phosphorylation (an mTORC1 target) is inhibited by *MLST8* deletion (Fig. 1C). Pretreatment with the mTOR kinase inhibitor Torin1 (100 nM) inhibits both (Fig. 1C), confirming that mLST8 loss specifically disrupts mTORC2. Both RICTOR and BioID2-RICTOR containing mTORC2 complexes also have a similar IC₅₀ for Torin1 (6.407 versus 5.747 nM for control and BioID2-RICTOR cells, respectively) (Fig. 1D). These data confirm that BioID2-RICTOR forms functional mTORC2 complexes and that these complexes are disrupted by mLST8 loss without affecting BioID2-RICTOR expression or its interaction with SIN1.

BioID2-RICTOR proximity labeling detects both known and novel interactions

To identify proteins proximal to mTORC2 in living cells, 50 μM biotin was supplemented into the culture medium of actively growing control, BioID2-RICTOR, and BioID2-RICTOR^{mLST8Δ} cells. After a 24 h incubation period, biotinylated proteins were purified using streptavidin-conjugated resin, eluted, and identified by LC-MS (Fig. S1C and Experimental procedures). For each labeling experiment, individual peptide counts and protein abundances (iBAQ values) were calculated based on their prevalence in three technical replicates for each individual cell line. Complete proximity labeling experiments were performed twice with each clonal line and for each cell type (control, BioID2-RICTOR, and BioID2-RICTOR^{mLST8Δ}), totaling four biological replicates for each of the three conditions, thus allowing for high stringency in setting cutoffs for positive interactions.

Protein interactions were considered “high confidence” if >1 peptide was present in at least three of four replicates and in no controls, “medium confidence” if >1 peptide was present in two replicates or one peptide was present in multiple replicates and in no controls, and “fair confidence” if peptides were enriched (iBAQ experimental/control >10) in at least two replicates of experimental samples compared to control samples (Table S1). An interacting protein was considered mTORC2-dependent if it was more abundant in BioID2-RICTOR cells compared to BioID2-RICTOR^{mLST8Δ} cells by

> 2-fold. These criteria identified 52 high, 118 medium, and 45 fair confidence RICTOR-interacting proteins (215 total interactions). Of these, 181 proteins were mTORC2 dependent (detected in BioID2-RICTOR cells but not in control or BioID2-RICTOR^{mLST8Δ}) (Fig. 2A), indicating that most of the BioID2-RICTOR protein interactions require intact mTORC2.

Applying STRING (Search Tool for the Retrieval of Interacting Genes/Proteins) analysis to the BioID2-RICTOR interactome reveals more edges (704) than would be expected (369) from an unrelated protein interaction list ($p = 1 \times 10^{-16}$), indicating significant connectivity among proteins within the BioID2-RICTOR interactome (Fig. S2). Importantly, the mTORC2 subunits RICTOR, SIN1, PRR5, and PRR5L were detected in BioID2-RICTOR cells (Fig. 2B and Table S2). RICTOR and SIN1, but not the other mTORC2 components, were also detected in BioID2-RICTOR^{mLST8Δ} cells (Fig. 2B), consistent with RICTOR and SIN1 interacting independent of mTORC2 assembly (Fig. 1A). There was no mTOR labeling detected in any samples; however, structural studies suggest mTOR is out of range of the BioID2 tag (21) and may not have lysine residues accessible to the BirA biotin ligase. These data provide strong validation of the strategy.

Gene ontology analysis of biological function of the 181 mTORC2-dependent proteins indicates mRNA splicing, cell cycle control, chromatin dynamics, TOR signaling, and DNA repair among the over-represented functional classes (Fig. 2C). Among the mTORC2-dependent BioID2-RICTOR interactome, 44% of the proteins (80) also have known connections to mTORC2 (Fig. 2D and Table S2). For example, 32 protein interactors have previously been reported to co-IP with either RICTOR, SIN1, mTOR, or mLST8, 8 are reported regulators of an mTORC2 subunit, 15 interact with AKT, and 25 regulate AKT S473 phosphorylation (Fig. 2D and Table S2). In addition, eight proteins in the BioID2-RICTOR interactome share a previously reported common interacting protein with RICTOR (Fig. 2E and Table S2). For example, RICTOR interacts with BRCA1 (23), which forms the BRCA1-A complex with the RICTOR-interacting protein UIMC1 (RAP80) identified in this study. These previous connections are further annotated in Table S2. The identification of biologically meaningful mTORC2 interactions demonstrates that this technique successfully elucidates functional mTORC2 connections in disparate biological pathways.

BioID2-RICTOR interacting proteins are cytoplasmic and nuclear

The high number of BioID2-RICTOR interactor proteins that have functional roles in a nuclear biological process (e.g., RNA splicing, chromatin remodeling, DNA damage repair) was unexpected. Moreover, classifying the BioID2-RICTOR interactome by predicted intracellular localization indicates that 47 interactors are exclusively nuclear, and 90 interactors are both nuclear and cytoplasmic (Figs. 3A and S3A). We recently observed a pool of nuclear RICTOR in brown adipocytes (24), while other studies reported nuclear RICTOR in

Endogenous RICTOR/mTORC2 proximity labeling

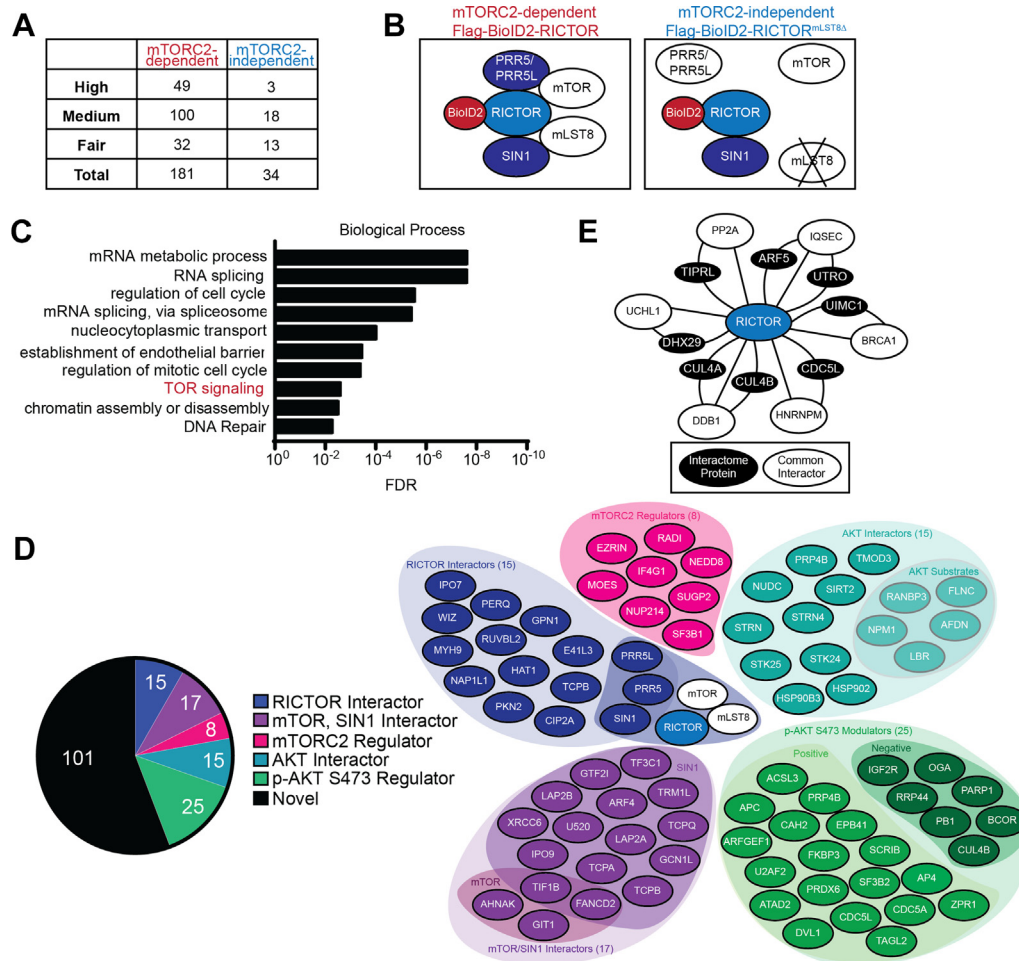


Figure 2. BioID2-RICTOR interactome identifies known and novel mTORC2 interactors and functions. *A*, table showing the number of proximal proteins for each confidence level in Flag-BioID2-RICTOR (mTORC2 dependent, *red*) and Flag-BioID2-RICTOR^{mLST8Δ} (mTORC2 independent, *blue*) after data processing from $N = 4$ separate experiments. *B*, mTORC2 components that appear in the BioID2-RICTOR interactome with or without mLST8. Biotin-labeled proteins shown in *blue*; unlabeled proteins are shown in *white*. *C*, gene ontology of the mTORC2-dependent interactome demonstrating TOR signaling as one of the *top* significant hits as well as several nuclear processes (RNA processing/splicing, nucleocytoplasmic transport, chromatin changes, and DNA repair) and cytoplasmic processes (cell cycle regulation and establishment of endothelial barrier). FDR, false discovery rate. *D*, pie graph showing that 80 interactors have previously been associated with mTORC2 components, AKT, or AKT activation (phosphorylation of S473). These interactors are plotted below in different regions corresponding to their previously reported functions. The *dark blue* center cloud indicates mTORC2 components. *White* proteins are those not labeled by BioID2-RICTOR. *E*, interactome proteins (*black*) that share a common interactor (*white*) with RICTOR. Straight lines represent previously published interactions. Curved lines represent novel interactions discovered in this RICTOR interactome study.

fibroblasts (25) and prostate cancer cells (26). To determine the broader relevance of these observations, we fractionated our clonal HEK293E cells as well as MCF7 breast cancer, A549 lung adenocarcinoma, Panc1 pancreatic cancer, and U87 glioblastoma cells and probed for mTORC2 subunits in the cytoplasm and the nucleus. In all cases, a fraction of the total RICTOR, mTOR, and SIN1 (α isoform) protein was detectable in the nuclear fraction (Fig. 3, *B* and *C*). Additionally, we examined HEK293E cells following serum deprivation and stimulation conditions (Fig. S3*D*) and did not observe changes in nuclear Rictor localization, suggesting growth factor signaling does not influence Rictor translocation, at least under the conditions tested here. Consistently, immunostaining for endogenous RICTOR (27) suggests 39% of total RICTOR is in the nucleus (Fig. S3, *A* and *B*), while transiently expressing YFP-RICTOR similarly indicates 30% to 40% of the total YFP-RICTOR is nuclear, independent of mLST8 (Fig. 3,

D–F). These data are consistent with RICTOR/mTORC2 being present in the nucleus of many cell types.

The mTORC2-independent BioID2-RICTOR interactome indicates RICTOR associates with the ribosome

How RICTOR might function independent of its association with mTORC2 is unclear. Only 34 interacting proteins (32 in addition to BioID2-RICTOR itself and SIN1) passed the stringency cutoff in BioID2-RICTOR^{mLST8Δ} cells, which cannot form mTORC2 complexes (Fig. 1*A*). Both cytoplasmic and nuclear proteins are among these mTORC2-independent RICTOR interactors (Fig. S3*C*). Interestingly, 8 of these proteins (24%) are ribosomal proteins (Fig. S3*C*). Previous studies suggest an interaction between mTORC2 and the ribosome (28, 29). The enrichment of ribosomal proteins in the BioID2-RICTOR^{mLST8Δ} interactome may indicate a role for mTORC2

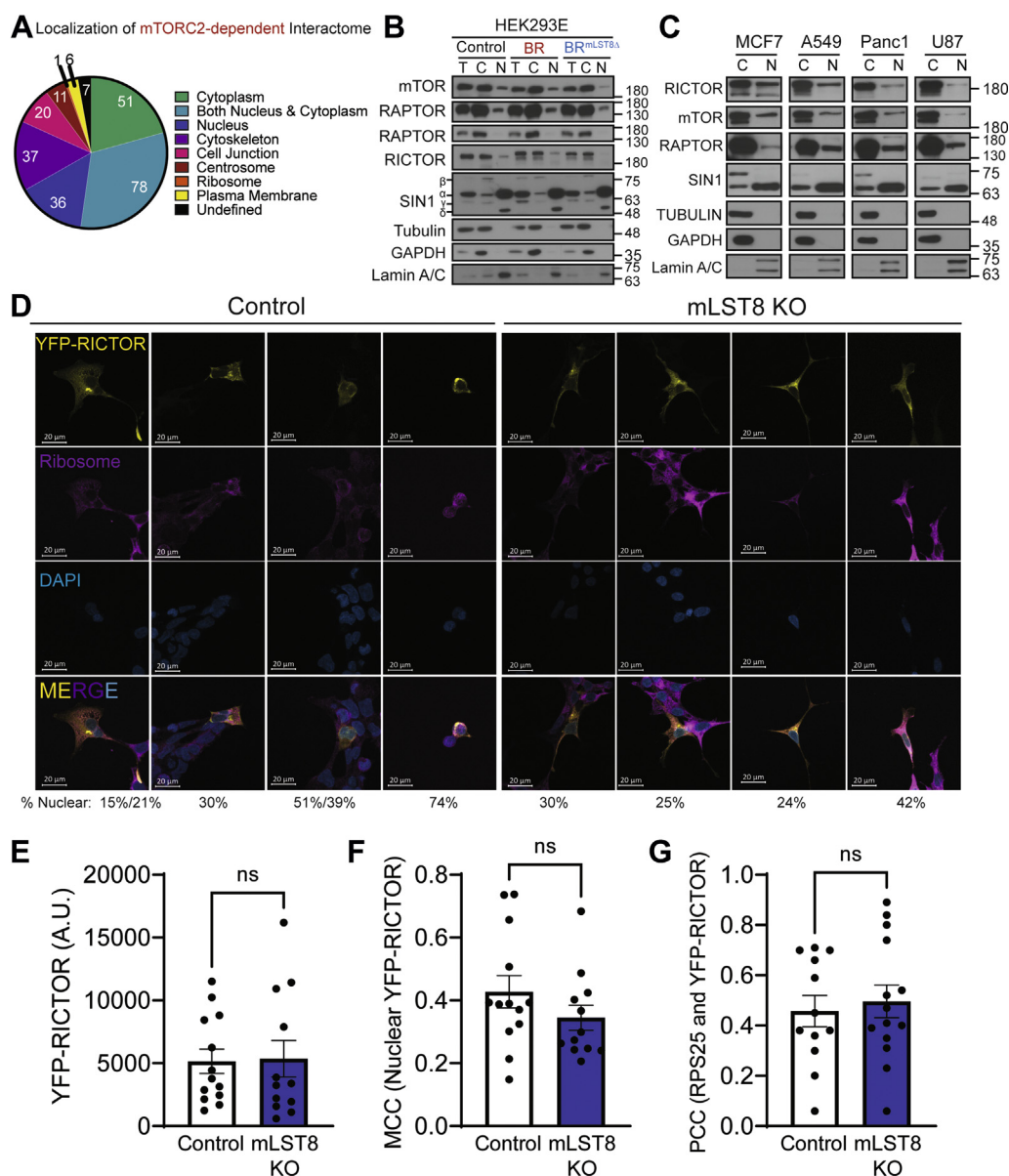


Figure 3. Flag-BioID2-RICTOR localization and subcellular localization of its interactors. *A*, pie chart of the localization of the mTORC2-dependent RICTOR interactors. *B*, cytoplasmic and nuclear fractionation of HEK293E cells. T, total cell lysate; C, cytoplasm; N, nuclear. BR = Flag-BioID2-RICTOR. SIN1 isoforms are labeled according to Frias *et al.* (65). N = 3. *C*, cytoplasmic and nuclear fractionation of four cancer cell lines. N = 4. *D*, immunofluorescence of YFP-RICTOR overexpressed in HEK293E cells costained with RPS25 ribosomal marker and DAPI nuclear marker. The scale bar represents 20 μ m. *E*, total YFP-RICTOR expressed per cell in arbitrary units (A.U.). *F*, Mander's colocalization coefficient for YFP-RICTOR that appears in the nucleus of each cell. N = 13, 12. ns, not significant. *G*, Pearson correlation coefficient corresponding to the amount of overlap between YFP-RICTOR and RPS25.

in determining ribosome abundance or an increased affinity for free RICTOR (independent of mTORC2) for ribosomes. The amount of ribosomal protein RPL4 and RPS25 is unaffected by mLST8 loss (Fig. S3F) arguing against increased ribosome abundance. We also colocalized RICTOR and the ribosomal protein RPS25 with and without mLST8. The Pearson coefficient in control cells is 0.45 ± 0.22 and the mLST8 KO cells is 0.50 ± 0.24 , indicating the association between RICTOR and RPS25 is unaffected by mLST8 (Fig. 3G). Because RICTOR in mLST8-deficient cells associates with ribosomes at about the same amount as RICTOR that can complex with mTOR, we reason that RICTOR may be able to associate with ribosomes outside of the mTORC2 complex.

BioID2-RICTOR interacting proteins contain insulin-sensitive, Rictor-dependent phosphorylation sites

We next crossreferenced the BioID2-Rictor interactome with four published proteomics datasets from studies investigating either mTOR-sensitive phosphorylation sites (30, 31), Rictor-dependent phosphorylation sites (32), or insulin-stimulated phosphorylation sites (Fig. 4A) (33). Intriguingly, 86 BioID2-RICTOR interacting proteins appear in one or more of these studies (Table S3). For example, 13 BioID2-RICTOR interacting proteins contain phosphorylation sites sensitive to an mTOR kinase inhibitor and at least 8 of these phosphoproteins are also Rictor dependent (Fig. 4A and Table S4) (30–32).

Endogenous RICTOR/mTORC2 proximity labeling

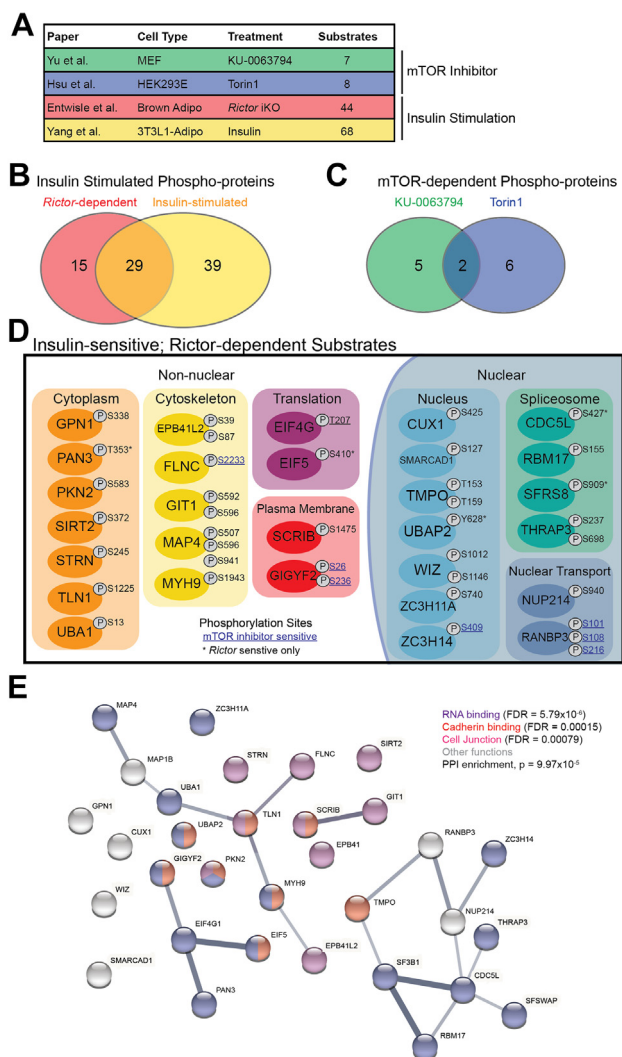


Figure 4. Interactome proteins that have mTOR, Rictor, or insulin-dependent phosphosites. A, summary of four previous phosphoprotein datasets used is analyzed in this figure. B, Venn diagram showing the overlap of BioID2-RICTOR interactome proteins that appeared in the insulin-stimulated (yellow) and Rictor KO phospho-proteomes (red). C, Venn diagram showing the overlap of BioID2-RICTOR interactome proteins that appeared in the two mTOR inhibitor studies. D, phosphoproteins that are both insulin sensitive and Rictor dependent (overlap between red and yellow ovals from B). Proteins were separated by localization and function. Each phosphosite is represented with a P in a gray circle. Those that are not shared between insulin sensitive and Rictor dependent have an asterisk after them. The phosphosite text that is blue and underlined represents phosphosites that also overlap with one of the mTOR inhibitor studies. E, STRING diagram of potential mTORC2 substrates that are dependent on both RICTOR and insulin. These are significantly enriched for RNA binding, cadherin binding, cell junction proteins, which are color coordinated accordingly. This protein List is also found in Table S4.

Remarkably, 68 BioID2-RICTOR interacting proteins contain an insulin-sensitive phosphorylation site (Fig. 4B). Among these sites, 29 are also Rictor dependent, 8 are sensitive to an mTOR kinase inhibitor, and 5 are Rictor dependent and sensitive to an mTOR kinase inhibitor (Fig. 4, B and C) (30–32). The 29 insulin-sensitive and Rictor-dependent phosphoproteins were examined more closely to determine if the phosphorylation sites observed were conserved across both studies. This showed that 82% (24/29) have at least one common phospho site shared under conditions of insulin

stimulation and Rictor loss. These may reflect mTORC2 substrates or substrates phosphorylated by other kinases in the PI3K/mTOR pathway and should be investigated in the future. Examining the subcellular localization category (Uniprot) of these proteins finds that approximately half are predominantly nuclear and half are predominantly cytoplasmic or cytoskeletal. Interestingly, several of these phosphoproteins are important for different steps of mRNA processing by the spliceosome (Figs. 2C, 4, D and E). These phosphoproteins are also enriched for cadherin binding, which occurs at the plasma membrane, and cell junctions which could reflect a role for mTORC2 in barrier function and cell permeability (Fig. 4E). These data suggest new spatial connections of mTORC2 to the insulin-stimulated phosphoproteome.

ARF1 is a RICTOR-interacting protein that attenuates mTORC2 signaling

BioID2-RICTOR interacting proteins were also classified by enzymatic function, which includes proteins with defined functional domains (e.g., kinase, phosphatase, GTPase, acetyltransferase) and proteins that regulate these enzymes (e.g., GTPase activating proteins and exchange factors) in the analysis. This uncovered 48 proteins classified by kinase (n=12), phosphatase (n=4), acetylation/deacetylation (n=8), methylation/demethylation (n=6), GTPase (n=10), or ubiquitination (n=8) pathway function (Fig. 5A). Among these proteins, we identified nodes of interaction. These include the following: a sterile-20-like kinase network containing the MST4, STK24, and STK24 kinases and a phosphatase regulatory subunit (Fig. S4A); a chromatin remodeling node containing HAT1, RBBP4, RBBP7, TRIM28, SMARCAD1, and SIRT2 (Fig. S4B); and a ubiquitination network containing NEDD8, UBE2M, CUL4A, CUL4B, DCAF7, and FBOX30 (Fig. S4C). Notably, treating cells with the NEDD8 activating enzyme 1 (NAE1) inhibitor MLN4924 (which blocks transfer of NEDD8 to UBE2M) increases the level of RICTOR and its known substrates CUL4A/B (34) (Fig. S4, D and E). Treating cells with the proteasome inhibitor MG132 alone has no effect on Rictor levels (Fig. S4F). Overexpressing His-UBE2M (which transfers NEDD8 to substrates) conversely decreases RICTOR levels (Fig. S4E). Additionally, overexpressed His-UBE2M interacts with RICTOR and mTOR by co-IP (Fig. S4H), collectively suggesting the NEDD8 pathway may contribute to mTORC2 regulation.

Particularly interesting among the enzyme RICTOR interactors is the identification of a GTPase network containing the ARF1, ARF3, and ARF5 GTPases, the ARFGEF1 and ARFGEF2 guanine nucleotide exchange factors, and the GTPase-activating protein GIT1 (Fig. 5B). The ADP ribosylation factor (ARF) family GTPases are small guanine nucleotide-binding proteins in the RAS superfamily best known for roles in vesicle trafficking (35, 36). ARFGEFs activate ARF proteins by promoting ARF GDP exchange for GTP (36), and GIT1 is a GTPase-activating protein that stimulates ARF GTP hydrolysis (36). Overexpression of ARF1-HA in HEK293E cells and pulldown with the HA antibody demonstrates that ARF1

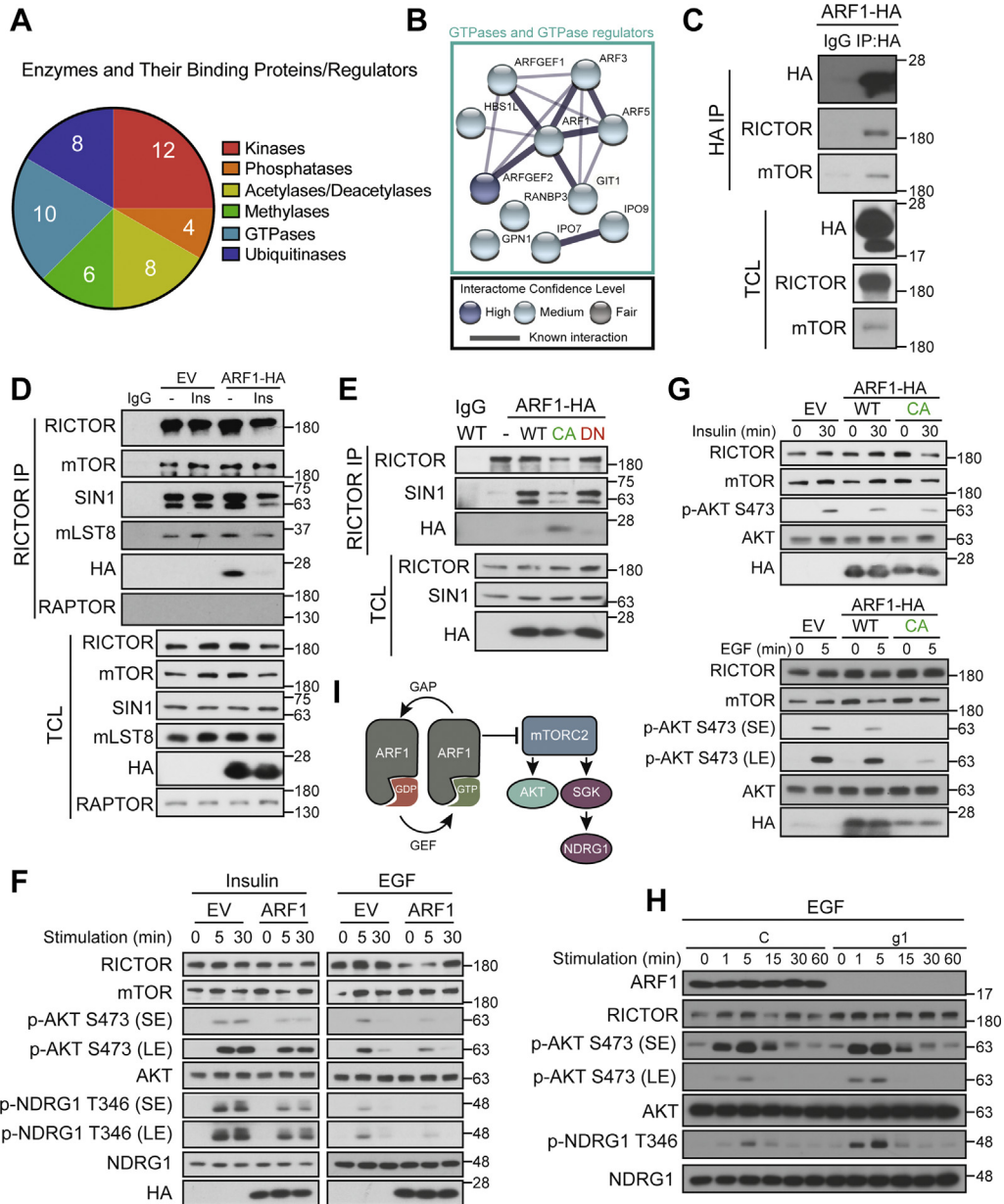


Figure 5. ARF1 binds with mTORC2 and dampens mTORC2 signaling. *A*, pie chart of the BiID2-RICTOR interactome categorized by enzymes and their regulators. Numbers within the chart are actual numbers of proteins in each category. *B*, STRING diagram of GTPases and their regulators in the RICTOR interactome. Circles represent the proteins and connecting lines represent previously known interactions (thicker corresponds to amount of evidence in the literature). *C*, immunoprecipitation of overexpressed HA-tagged ARF1 with mTOR and RICTOR. TCL, total cell lysate. *N* = 3. *D*, RICTOR IP of ARF1 from serum deprived (-) and 30 min insulin-stimulated (Ins) conditions. ARF1 binds more strongly with RICTOR and mTOR when the cells are in a serum-deprived state. *N* = 3. *E*, ARF1-CA (GTP bound) binds more strongly with RICTOR than ARF1 or ARF1-DN (GDP bound). CA, constitutively active; DN, dominant negative. *N* = 3. *F*, insulin (left) and EGF (right) time course in empty vector (EV) or ARF1-HA expressing cells. Overexpression of ARF1-HA inhibits maximal mTORC2 signaling stimulated by insulin/EGF. *N* = 4. *G*, GTP-bound ARF1 inhibits maximal mTORC2 signaling stimulated by insulin (top) or EGF (bottom). *N* = 3. *H*, CRISPR KO of *Arf1* enhances maximal EGF-stimulated AKT and NDRG1 phosphorylation. Cells were serum deprived then stimulated with EGF over a time course. Results were confirmed with two independent guides (Fig. S5). Model of ARF1 inhibition of mTORC2 through direct binding to the complex when it is in its GTP-bound state during serum-starved conditions. All experiments were done in HEK293E cells. IP, immunoprecipitation.

binds with both RICTOR and mTOR (Fig. 5C). This interaction with ARF1 is growth factor modulated. Endogenous RICTOR co-IPs with the mTORC2 components mTOR, SIN1, and mLST8 under both serum deprivation (5 h) and insulin stimulation (30 min, 10 nM); however, ARF1-HA is only detectable in RICTOR immunoprecipitations (IPs) under serum deprivation (Fig. 5D). GTP-bound ARF1 better associates with membranes (37, 38) and often ARFs interact with

their targets in their active state (39), so we tested if being in a GTP-bound state increases the RICTOR-ARF1 interaction. To this end, we overexpressed ARF1-HA, constitutively active ARF1-HA (Q71L) (CA), or dominant negative ARF1-HA (T31N) (DN) and performed endogenous RICTOR IP under basal medium conditions that destabilize RICTOR binding to WT ARF1-HA (Fig. 5E). In these experiments, constitutively active but not dominant negative ARF1 co-IPs with

Endogenous RICTOR/mTORC2 proximity labeling

endogenous RICTOR consistent with GTP-bound ARF1 more stably associating with immunopurified mTORC2 complexes.

We next asked whether ARF1 functionally regulates mTORC2 signaling by gain and loss of function analysis. First, we find that overexpressing ARF1-HA attenuates both insulin- and EGF-stimulated AKT S473 as well as NDRG1 T346 phosphorylation *via* SGK compared to expressing of empty vector (Fig. 5F). Moreover, overexpressing constitutively active ARF1-HA (Q71L) has an even greater inhibitory effect especially on EGF-stimulated AKT S473 phosphorylation compared to WT ARF1-HA (Fig. 5G). Next, we deleted *Arf1* by CRISPR-Cas9 genome editing to ask whether losing ARF1 enhances EGF signaling. Indeed, in an EGF1 stimulation time course, deleting *Arf1* with either of two unique guides enhances both AKT S473 and NDRG1 T346 phosphorylation within 5 min post stimulation, when the signaling response is maximally induced (Figs. 5H and S5). Collectively, these data suggest a model in which ARF1 is proximal suppressor of mTORC2 (Fig. 5I).

Discussion

Protein interaction networks help define the regulatory landscape of a particular protein or protein complex. Because the regulation and intracellular localization of mTORC2 is not well understood, we developed a BioID2-based proximity labeling strategy to map the endogenous RICTOR/mTORC2 protein interaction network in living cells. Our approach uncovered an extensive list of known and novel RICTOR-interacting proteins highlighting potential connections between mTORC2 and both known and novel cytoplasmic and nuclear processes. Overall, we provide both a method of tagging endogenous mTORC2 and a detailed resource of RICTOR-interacting proteins that can be further used to uncover biologically meaningful mTORC2 regulatory networks and functions.

A main advantage of BioID2 proximity labeling is the ability to identify protein interactions that occur in living cells. This can overcome the challenge of detecting weak or transient interactions that are often difficult to maintain in more traditional protein interaction discovery methods such as affinity purification MS. Another advantage of our strategy is the use of CRISPR engineering to insert the BioID2 proximity labeling enzyme into the *RICTOR* genomic locus, thus maintaining *RICTOR* gene expression from its endogenous promoter and regulatory elements. In theory, a similar strategy could be performed by tagging endogenous Sin1; however, N-terminal Sin1 could not be tagged probably because it disrupts protein function. The existence of multiple Sin1 isoforms with variable ends poses a challenge to tagging the endogenous C terminus. Regarding cell line choice, we selected human embryonic kidney cells both because they are amenable to CRISPR engineering and because they have been used extensively to study the mTOR complexes. The fact that nearly half of the BioID2-RICTOR interacting proteins we discovered have a connection in the literature to mTORC2 signaling supports the overall reliability of this strategy, though rigorous

follow-up of each interaction detected is required to confirm individual functional relevance.

It is interesting that 20% of the BioID2-RICTOR interacting proteins exclusively localize to the nucleus. While it is possible that BioID2-RICTOR could interact with these proteins in the cytoplasm or transiently following nuclear envelope breakdown during mitosis, nuclear localization of mTORC2 subunits is observed in this study, and previously by others in HEK293, IMR-90, and NIH3T3 cells (25, 40). Consistent among this and previous studies is that only a fraction of the total cellular amount each mTORC2 core component (*i.e.*, mTOR, RICTOR, SIN1) is nuclear (*i.e.*, ~30% for RICTOR) and nuclear RICTOR does not depend on mLST8 or growth factor signaling. However, a nuclear function for mTORC2 has yet to be defined. In *Schizosaccharomyces pombe*, TORC2 functions in genome stability and recovery from DNA damage repair (41). Thus, it is interesting that 16 BioID2-RICTOR interacting proteins function in the DNA damage response pathway. If and how mTORC2 translocates to the nucleus and functions in nuclear processes warrants further investigation.

Many BioID2-RICTOR interacting proteins contain phosphorylation sites sensitive to an agonist (*e.g.*, insulin) and/or antagonists (*e.g.*, mTOR kinase inhibitors, *Rictor* deletion) of mTORC2 kinase activity. Because AKT positively regulates mTORC1, some of BioID2-RICTOR interacting phosphoproteins could be direct substrates of either mTORC2 or mTORC1 (42–44). One example of an mTORC2 substrate in our dataset is the AGC family kinase PKN2, which was recently shown to be phosphorylated by mTORC2 in its turn motif (45, 46). Another possibility is that interacting phosphoproteins function downstream in the mTORC2 signaling cascade. For instance, FLNC (47) and RANBP3 (Fig. 4D) are AKT substrates, the latter of which regulates nuclear transport (48). It is also possible that some of these phosphoproteins require active mTORC2 in a different kinase or phosphatase pathway. Although the phospho-proteomics datasets that we crossreferenced our dataset with were generated in different cell types (MEFs, HEK293E, brown adipocytes, 3T3L1 adipocytes) (Fig. 4A), the resultant phosphoprotein mTORC2 interactome is likely an under representation of what is biologically important. For example, AKT2 and AKT3 were identified as medium confidence BioID2-RICTOR interacting proteins in only one biological replicate of the interactome studies (Table S1), excluding AKT from the final high-stringency list and from the list of substrates obtained. Nevertheless, these data provide new insight into the phospho-proteomics landscape proximal to mTORC2 and may indicate the presence of mTORC2 signaling hubs at new subcellular places like the cytoskeleton or spliceosome.

This study also identified potential novel mechanisms of RICTOR/mTORC2 regulation. For example, the finding that UBE2M interacts directly with RICTOR, mTOR, and to a lesser extent with RAPTOR (Fig. S4G) suggests it may balance the protein levels and/or activity of mTORC2 and mTORC1. Consistently, the Cullin4 (CUL4) E3 ligases, which require UBE2M-dependent neddylation to become active, reportedly regulate the mTOR complex inhibitor protein DEPTOR (34)

and bind with RAPTOR and mLST8 (49). More commentary on a potential mechanism is included in Fig. S4. The BioID2-RICTOR interactome also contained DCAF7, a substrate receptor protein for the CUL4 ligases. Interestingly, the *Wnt1-Cre;Rictor1/l* mouse (*Mus musculus*), which has *Rictor* deleted in the neural crest, and the *dcaf7*^{-/-} zebrafish (*Danio rerio*) share a similar pattern of craniofacial dysmorphia (50, 51), indicating overlapping biological function in development.

The ARF1 GTPase was also identified as a proximal RICTOR protein that may regulate mTORC2. Our BioID2-RICTOR interactome additionally includes GEFs (ARFGEF1, ARFGEF2) and a GAP (GIT1). ARF1 has previously been implicated in AKT signaling (52, 52–55); however, the mechanism is unknown. ARF1 may translocate to the plasma membrane upon insulin signaling (56) and bind the insulin receptor (54), possibly functioning in receptor trafficking by endocytosis. A recent publication also found that mTORC2 localization to endosomes is required for its signaling activity in glioma cells (57). Thus, regarding the mechanism of mTORC2 suppression by ARF1, one hypothesis is that ARF1 encounters mTORC2 on endosomes to help downregulate mTORC2/AKT activity, possibly by disrupting mTORC2 localization or substrates interactions, following receptor stimulation and internalization. ARF1 overexpression could also enhance the kinetics of receptor trafficking, turnover from the membrane to endosomes, where receptor-mediated signaling is turned off, or Golgi–endoplasmic reticulum trafficking, which is also regulated by ARFs. Another possibility is that ARF1 suppresses mTORC2 kinase activity by directly inhibiting its catalytic activity. If this is the case, understanding the mechanism will require detailed structural information about the interaction. Notably, ARF3 and ARF5 are also Rictor proximal proteins raising the possibility that there is compensatory function between different ARFs. Whether receptor internalization or Golgi–endoplasmic reticulum trafficking is required for ARF1 to attenuate mTORC2 signaling and other details of the mechanism are important areas for future investigation.

There are some limitations of this study. One disadvantage of using BioID2 is that the labeling period is 12 to 24 h long. While this increases the chances of detecting a transient interaction, it may also increase the chance of nonspecific interactions. Setting stringent cutoffs for MS data, stratifying the interactome by confidence, and including an *MLST8* KO control help mitigate against false positive interactors. Moreover, newer BioID2 variations, such as TurboID, which can label interacting proteins within minutes, can be used in the future to circumvent this caveat, especially when combined with acute treatments that affect mTORC2 signaling, such as growth factor stimulation. The BioID2 tag itself is 26 kDa in size and placing any epitope tag on a protein could disrupt certain interactions. BioID2 labeling also requires that a protein have a lysine residue exposed in the labeling radius, which may not be the case for all real interactors. Finally, our strategy is also limited to the interactions that exist in the clonal cell lines we used. It is important that novel interactions identified are

validated in diverse cell types and with endogenous proteins for determining functional relevance.

To conclude, we developed a method of tagging endogenous mTORC2 and mapping its proximal protein interaction network in living cells. This strategy can be applied with other epitope tags while the protein interaction network generated here can guide future investigations into mTORC2 regulation, including by ARF1.

Experimental procedures

Cell lines

HEK293E, PANC-1, HeLa, U87, and MCF7 cells were grown in 5% CO₂, humidity at 37 °C in 10% fetal bovine serum (FBS), penicillin/streptomycin, Dulbecco's modified Eagle's medium. A549 cells were grown in 5% CO₂, humidity at 37 °C in 10% FBS, penicillin/streptomycin, RPMI. All cell lines were originally from ATCC, used up to a maximum of 15 passages, and routinely checked for *mycoplasma* contamination. Clonal HEK293E cells with Flag-BioID2-RICTOR tag were authenticated by sequencing the region upstream and downstream of the *RICTOR* start site for correct insertion of the tag and by band shift on Western blot using Flag and RICTOR antibody. *MLST8* deletion was verified by its absence by Western blot.

Cloning and knock-in cell generation

pX330 Cas9-Puro targeting the *RICTOR* start codon with the sequence 5'-ACTGAAACCCGTCAATATGG-3' was transfected in with pBABE-donor where the donor plasmid was comprised of and 427 bp 5' homology arm, a 3×Flag tag, the BioID2 tag, a flexible linker made of 3×GGGS repeats, and a 371 bp 3' homology arm. Cells were selected with puromycin for 2 days and then individual colonies were grown until there were enough cells for genotyping and Western blot. Individual clones were checked for protein expression and their *RICTOR* genomic locus was PCR amplified and sequenced.

Proximity labeling

About 3 × 15 cm dishes were used for each replicate. Briefly, cells were grown to ~90% confluence in 10% FBS and 1% penicillin/streptomycin (complete media). Then they were treated with 50 μM biotin in complete media for 24 h. Cells were lysed in a 1% Triton buffer, sonicated, and immunoprecipitated overnight in streptavidin magnetic beads (NanoLink). These were washed 4 × 8 min each in a series of buffers as described (58). They were eluted in 10 mM biotin, 50 mM Tris, pH 8.0, 2% SDS, and boiled off the beads. Samples were frozen until their final preparation to precipitate them to be cleaned of SDS and run on MS.

Label-free LC-MS/MS analysis

Pull downs were analyzed on a Q-Exactive Plus quadrupole Orbitrap mass spectrometer (ThermoScientific) equipped with an Easy-nLC 1000 (ThermoScientific) and nanospray source (ThermoScientific). Peptides were resuspended in 5% methanol/1% formic acid and loaded on to a trap column (1 cm length, 100 μm inner diameter, ReproSil, C18 AQ 5 μm 120 Å

Endogenous RICTOR/mTORC2 proximity labeling

pore [Dr Maisch, Ammerbuch, Germany]) vented to waste *via* a microtee and eluted across a fritless analytical resolving column (35 cm length, 100 μ m inner diameter, ReproSil, C18 AQ 3 μ m 120 \AA pore) pulled in-house (Sutter P-2000, Sutter Instruments) with a 45 min gradient of 5% to 30% LC-MS buffer B (LC-MS buffer A: 0.0625% formic acid, 3% acetonitrile; LC-MS buffer B: 0.0625% formic acid, 95% acetonitrile). The Q-Exactive Plus was set to perform an Orbitrap MS1 scan ($R = 70K$; AGC target = $1e6$) from 350 to 1500 m/z , followed by higher-energy collisional dissociation (HCD) MS2 spectra on the 10 most abundant precursor ions detected by Orbitrap scanning ($R = 17.5 K$; AGC target = $1e5$; max ion time = 50 ms) before repeating the cycle. Precursor ions were isolated for HCD by quadrupole isolation at width = 1 m/z and HCD fragmentation at 26 normalized collision energy. Charge state 2, 3, and 4 ions were selected for MS2. Precursor ions were added to a dynamic exclusion list ± 20 ppm for 15 s. Peak lists were generated using in-house developed software Rthur 1.0. Raw data were searched using COMET (release version 2014.01) in high resolution mode (59) against a target-decoy (reversed) (60) version of the human proteome sequence database (UniProt; downloaded 2/2013, 40,482 entries of forward and reverse protein sequences) with a precursor mass tolerance of ± 1 Da and a fragment ion mass tolerance of 0.02 Da and requiring fully tryptic peptides (K, R; not preceding P) with up to three miscleavages. Static modifications included carbamidomethylcysteine and variable modifications included oxidized methionine. Searches were filtered using orthogonal measures including mass measurement accuracy (± 3 ppm), Xcorr for charges from +2 through +4, and dCn targeting a $< 1\%$ false discovery rate at the peptide level. Quantification of LC-MS/MS spectra was performed using MassChroQ (61) and the iBAQ method (62).

Interactome data analysis

Two separate clones of Flag-BioID2-Rictor HEK293E cells and mLST8 KO clones derived from each of these clones were used in two independent experiments each ($n = 4$ total). First, the interactors were ranked within each experiment as 1 (most confident/enriched) to 3 (less confident/enriched) by the following.

1. > 1 peptide in multiple replicates, 0 peptides in control
2. 1 peptide in multiple replicates, 0 peptides in control
3. > 1 peptide in multiple replicates, 1 peptide in 1 control replicate, iBAQ experimental/control > 10

Then these ranked lists (1–3) from each of the four independent experiments were compared. Interacting proteins were considered high confidence (1) interactors if they appeared as multiple peptides in multiple replicates in at least three of the four experiments and none in the controls, medium confidence (2) if they appeared as multiple peptides in multiple replicates in two experiments, and fair confidence (3) if they appeared enriched in experimental samples compared to control samples (iBAQ experimental/control > 10) in at least two experiments. The protein was considered mTORC2 dependent *versus* mTORC2 independent if the number of its

detected peptides was enriched by at least 2-fold. The list of total interactors was analyzed using STRING database (string-db.org), PANTHER DB, and ENRICHR gene ontology tools.

Western Blots

Ten to twenty micrograms of lysate was run on each Tris-Glycine SDS page gel of 8% to 16% depending on protein size. This was wet transferred onto polyvinylidene difluoride membranes and blocked with 5% milk, PBS with Tween-20, or 5% bovine serum albumin. Primary antibody incubations were done overnight (~ 16 h), rocking at 4 $^{\circ}\text{C}$. Secondary antibody was used at 1:10,000 (Cell Signaling) for 1 h, rocking at room temperature and visualized using Western Lightning ECL and developed on X-ray film. All antibodies used are listed in the Key resources table.

IP

A standard IP protocol was followed using an overnight incubation at 4 $^{\circ}\text{C}$ with antibodies in 40 mM Tris, pH 7.5, 120 mM NaCl, 1 mM EDTA, 0.3% CHAPS buffer with protease and phosphatase inhibitors (63), a 2 h incubation with protein A/G Sepharose (Prometheus), and elution by boiling in 2 \times SDS loading buffer. CHAPS and inhibitors were added fresh before usage. Leftover buffer was frozen and thawed when ready to use at a later time. N is at least 3 for each experiment.

CRISPR KO cells

LentiCRISPRv2 (Addgene #52961) virus that contains Cas9 and a guide RNA scaffold was used to transduce human cells for stable KO. The sequences for the guide RNAs were as listed in the Key Resources table. pX330 (Addgene #52961) was used for all transient use of CRISPR/Cas9 used in Flag-BioID2-RICTOR cell line generation. These guides are also listed in the Key Resources table.

Fractionation

Nuclear-cytoplasmic fractionation was completed as previously described (64). Briefly, the cytoplasmic fraction was collected in 20 mM Tris, pH 7.6, 20 mM MgCl_2 , 0.1 mM EDTA, 0.3% CHAPS buffer; the nuclei were collected by centrifugation, washed three times, and lysed in nuclear buffer containing 20 mM Hepes, pH 7.9, 400 mM NaCl, 2.5% glycerol, 1 mM EDTA, and 0.5 mM DTT. Then, the nuclei were frozen to -80 $^{\circ}\text{C}$ and thawed twice before spinning at 14K RPM, 4 $^{\circ}\text{C}$ to remove membranes and the insoluble fraction. Protease and phosphatase inhibitors were added to both buffers directly before use. N = 4 for each cell line.

Growth factor stimulation

Cells were grown to 70% confluence and transfected with plasmid DNA using the manufacturer's instructions with Lipofectamine 3000 (Invitrogen). The media was changed to the next day, and 36 h after transfection, the cells were serum starved for 5 h, then stimulated with insulin (10 nM) or EGF (100 ng/ml) for the indicated amount of times. Cells were then

collected in 0.3% CHAPS buffer (63), incubated on ice for at least 45 min, and centrifuged to remove membranes. $N = 3$ or 4 for all conditions. Torin1 treatment was 100 nM where the concentration is not variable.

Imaging

HA-YFP-RICTOR (Addgene # 73387) was transfected into HEK293E cells with either control guide RNA or mLST8 guide RNA in LentiCRISPRv2 plasmid. Alternatively, endogenous RICTOR was detected with RICTOR antibody (Cell Signaling #2114). About 24 to 36 h after transfection, the cells were fixed with paraformaldehyde, blocked in 4% bovine serum albumin, and stained with antibodies for RPS25 (HPA03180B) overnight and 4',6-diamidino-2-phenylindole for 5 min. After mounting, the slides were imaged on a Zeiss LSM900 with Airyscan 2 confocal microscope with 63 \times oil immersion objective. Zen Blue (Zeiss) software was used to measure the area of the nuclear region, whole cell area, and the mean intensity of YFP staining in both regions on orthogonal projects containing at least 10 Z-stack images taken at 0.25 μ M. The YFP in the nucleus was divided by the total cellular YFP to calculate the Mander's colocalization coefficient in at least 12 YFP-containing cells per condition from two separate biological replicates. Colocalization between RPS25 (ribosomes) and YFP-RICTOR was calculated using a Pearson correlation of each cell using the Coloc2 plugin for FIJI image analysis software (ImageJ v2).

Substrate analysis

Interactome list was compared to proteins whose phosphorylation was decreased in conditions where mTORC2 was inhibited (Torin1(30)/KU-0063794(31)) or lost (*Rictor* inducible KO (32)) or whose phosphorylation increased under insulin stimulation (33). Those proteins that overlapped as mTORC2-dependent RICTOR interactors and had phosphorylation sites meeting the aforementioned requirements were included. Each interactor that overlapped between *Rictor* sensitive and insulin sensitive were investigated in further detail by finding the shared and unique phosphorylation sites to each using supplemental tables from Entwisle *et al.* (32) and the website affiliated with Yang *et al.* (33) (www.maths.usyd.edu.au/u/pengyi/software/PUEL/mTOR_substrate_prediction_L1.htm). The sites were examined for previous kinase identification and conservation from mouse to human using Phosphosite.org.

Quantification and statistical analysis

All statistical analysis was completed in GraphPad Prism Version 9.2.0 (GraphPad Software). Each figure has relevant n (biological replicates) and any relevant statistical analysis has that information in the figure legend. In microscopy assays, n = number of cells analyzed per condition. All graphs depict mean \pm SEM, if applicable. Sample size estimation was not done. No data were excluded from an analysis. Where two conditions were compared, the statistical test used was an unpaired Student's t test with Mann–Whitney correction.

Where more than two groups were compared, a nonparametric paired one-way ANOVA was used.

Data availability

The raw mass spectrometry proteomics datasets were deposited in the MassIVE public repository, PXD029755 (password: p878) and will be made public upon publication. They can also be found at the website located in Table 5S.

Processed proteomics data and curated datasets are located in the supplemental tables, and all other data reported in this article will be shared by the lead contact upon request. Phospho-proteomics datasets used for analysis were taken from previously published studies which are listed in Table 5S and method details.

Any additional information required to reanalyze the data reported in this article is available from the lead contact upon request.

Supporting information—This article contains supporting information [Table 5S; (66–71)] and supplemental tables.

Acknowledgments—We would like to thank their lab members for helpful discussions. We would like to thank Adwait Godbole and Christofer Welsh who assisted in editing and reviewing the manuscript. Fig. S1 was made at BioRender.com (Agreement number NG246QKONI).

Author contributions—A. K. L., E. D. K., and D. A. G. conceptualization; A. K. L., E. D. K., and S. M. J. methodology; A. K. L., E. D. K., and S. M. F. validation; A. K. L. and E. D. K. formal analysis; S. M. F., S. P. L., and A. N. K. investigation; A. K. L., E. D. K., S. P. L., and A. N. K. data curation; A. K. L. and D. A. G. writing—original draft; E. D. K., J. A. H., S. M. J., and A. N. K. writing—review & editing; A. K. L. and J. A. H. visualization; D. A. G. and A. N. K. supervision.

Funding and additional information—D. A. G. is supported by National Institutes of Health (NIH) grants R01CA196986, R01DK094004, and R01DK116005. A. N. K. is supported by NIH R35GM119455. A. K. L. was supported by an American Cancer Society Fellowship (PF-19-103-01-TBE). S. M. J. was supported by a postdoctoral fellowship from the American Diabetes Association (1-18-PDF-128). The content is solely the responsibility of the authors and does not necessarily represent the official views of the National Institutes of Health.

Conflict of interest—The authors declare that they have no conflicts of interest with the contents of this article.

Abbreviations—The abbreviations used are: co-IP, coimmunoprecipitation; FBS, fetal bovine serum; IP, immunoprecipitation; MS, mass spectrometry.

References

- Condon, K. J., and Sabatini, D. M. (2019) Nutrient regulation of mTORC1 at a glance. *J. Cell Sci.* 132
- Sancak, Y., Peterson, T. R., Shaul, Y. D., Lindquist, R. A., Thoreen, C. C., Bar-Peled, L., *et al.* (2008) The Rag GTPases bind raptor and mediate amino acid signaling to mTORC1. *Science* 320, 1496–1501

Endogenous RICTOR/mTORC2 proximity labeling

- Garcia-Martinez, J. M., and Alessi, D. R. (2008) mTOR complex 2 (mTORC2) controls hydrophobic motif phosphorylation and activation of serum- and glucocorticoid-induced protein kinase 1 (SGK1). *Biochem. J.* **416**, 375–385
- Sarbassov, D. D., Guertin, D. A., Ali, S. M., and Sabatini, D. M. (2005) Phosphorylation and regulation of Akt/PKB by the rictor-mTOR complex. *Science* **307**, 1098–1101
- Yan, L., Mieulet, V., and Lamb, R. F. (2008) mTORC2 is the hydrophobic motif kinase for SGK1. *Biochem. J.* **416**, e19–e21
- Qin, W., Cho, K. F., Cavanagh, P. E., and Ting, A. Y. (2021) Deciphering molecular interactions by proximity labeling. *Nat. Met.* **18**, 133–143
- Roux, K. J., Kim, D. I., Raida, M., and Burke, B. (2012) A promiscuous biotin ligase fusion protein identifies proximal and interacting proteins in mammalian cells. *J. Cell Biol.* **196**, 801–810
- Kim, D. I., Jensen, S. C., Noble, K. A., Kc, B., Roux, K. H., Mota-medchaboki, K., et al. (2016) An improved smaller biotin ligase for BioID proximity labeling. *Mol. Biol. Cell* **27**, 1188–1196
- Dumont, A. A., Dumont, L., Berthiaume, J., and Auger-Messier, M. (2019) p38alpha MAPK proximity assay reveals a regulatory mechanism of alternative splicing in cardiomyocytes. *Biochim. Biophys. Acta Mol. Cell Res.* **1866**, 118557
- Couzens, A. L., Knight, J. D., Kean, M. J., Teo, G., Weiss, A., Dunham, W. H., et al. (2013) Protein interaction network of the mammalian Hippo pathway reveals mechanisms of kinase-phosphatase interactions. *Sci. Signal.* **6**, rs15
- Che, Y., Siperashvili, Z., Kovalski, J. R., Jiang, T., Wozniak, G., Elcavage, L., et al. (2019) KRAS regulation by small non-coding RNAs and SNARE proteins. *Nat. Commun.* **10**, 5118
- Cui, Y., Groth, S., Troutman, S., Carlstedt, A., Sperka, T., Riecken, L. B., et al. (2019) The NF2 tumor suppressor merlin interacts with Ras and RasGAP, which may modulate Ras signaling. *Oncogene* **38**, 6370–6381
- Mirza, A. N., McKellar, S. A., Urman, N. M., Brown, A. S., Hollmig, T., Aasi, S. Z., et al. (2019) LAP2 proteins chaperone GLI1 movement between the lamina and chromatin to regulate transcription. *Cell* **176**, 198–212.e115
- Liu, G., Papa, A., Katchman, A. N., Zakharov, S. I., Roybal, D., Hennessey, J. A., et al. (2020) Mechanism of adrenergic CaV1.2 stimulation revealed by proximity proteomics. *Nature* **577**, 695–700
- Paeck, J., Kalocsay, M., Staus, D. P., Wingler, L., Pascolutti, R., Paulo, J. A., et al. (2017) Multidimensional tracking of GPCR signaling via peroxidase-catalyzed proximity labeling. *Cell* **169**, 338–349.e311
- Rhee, H. W., Zou, P., Udeshi, N. D., Martell, J. D., Mootha, V. K., Carr, S. A., et al. (2013) Proteomic mapping of mitochondria in living cells via spatially restricted enzymatic tagging. *Science* **339**, 1328–1331
- Hung, V., Lam, S. S., Udeshi, N. D., Svinkina, T., Guzman, G., Mootha, V. K., et al. (2019) Correction: proteomic mapping of cytosol-facing outer mitochondrial and ER membranes in living human cells by proximity biotinylation. *Elife* **8**, e50707
- Guertin, D. A., Stevens, D. M., Thoreen, C. C., Burds, A. A., Kalaany, N. Y., Moffat, J., et al. (2006) Ablation in mice of the mTORC components raptor, rictor, or mLST8 reveals that mTORC2 is required for signaling to Akt-FOXO and PKCalpha, but not S6K1. *Dev. Cell* **11**, 859–871
- Wang, T., Blumhagen, R., Lao, U., Kuo, Y., and Edgar, B. A. (2012) LST8 regulates cell growth via target-of-rapamycin complex 2 (TORC2). *Mol. Cell Biol.* **32**, 2203–2213
- Hwang, Y., Kim, L. C., Song, W., Edwards, D. N., Cook, R. S., and Chen, J. (2019) Disruption of the scaffolding function of mLST8 selectively inhibits mTORC2 assembly and function and suppresses mTORC2-dependent tumor growth *in vivo*. *Cancer Res.* **79**, 3178–3184
- Chen, X., Liu, M., Tian, Y., Li, J., Qi, Y., Zhao, D., et al. (2018) Cryo-EM structure of human mTOR complex 2. *Cell Res.* **28**, 518–528
- Scaiola, A., Mangia, F., Imseng, S., Boehringer, D., Berneiser, K., Shimobayashi, M., et al. (2020) The 3.2-A resolution structure of human mTORC2. *Sci. Adv.* **6**, eabc1251
- Krieger, K. L., Hu, W. F., Ripberger, T., and Woods, N. T. (2019) Functional impacts of the BRCA1-mTORC2 interaction in breast cancer. *Int. J. Mol. Sci.* **20**, 5876
- Jung, S. M., Hung, C. M., Hildebrand, S. R., Sanchez-Gurmaches, J., Martinez-Pastor, B., Gengatharan, J. M., et al. (2019) Non-canonical mTORC2 signaling regulates brown adipocyte lipid catabolism through SIRT6-FoxO1. *Mol. Cell* **75**, 807–822.e808
- Rosner, M., and Hengstschlager, M. (2008) Cytoplasmic and nuclear distribution of the protein complexes mTORC1 and mTORC2: rapamycin triggers dephosphorylation and delocalization of the mTORC2 components rictor and sin1. *Hum. Mol. Genet.* **17**, 2934–2948
- Audet-Walsh, E., Dufour, C. R., Yee, T., Zouanat, F. Z., Yan, M., Kalloghlian, G., et al. (2017) Nuclear mTOR acts as a transcriptional integrator of the androgen signaling pathway in prostate cancer. *Genes Dev.* **31**, 1228–1242
- Holla, S., Kurowska-Stolarska, M., Bayry, J., and Balaji, K. N. (2014) Selective inhibition of IFNG-induced autophagy by Mir155- and Mir31-responsive WNT5A and SHH signaling. *Autophagy* **10**, 311–330
- Zinzalla, V., Stracka, D., Oppliger, W., and Hall, M. N. (2011) Activation of mTORC2 by association with the ribosome. *Cell* **144**, 757–768
- Oh, W. J., Wu, C. C., Kim, S. J., Facchinetti, V., Julien, L. A., Finlan, M., et al. (2010) mTORC2 can associate with ribosomes to promote cotranslational phosphorylation and stability of nascent Akt polypeptide. *EMBO J.* **29**, 3939–3951
- Hsu, P. P., Kang, S. A., Rameseder, J., Zhang, Y., Ottina, K. A., Lim, D., et al. (2011) The mTOR-regulated phosphoproteome reveals a mechanism of mTORC1-mediated inhibition of growth factor signaling. *Science* **332**, 1317–1322
- Yu, Y., Yoon, S. O., Poulogiannis, G., Yang, Q., Ma, X. M., Villen, J., et al. (2011) Phosphoproteomic analysis identifies Grb10 as an mTORC1 substrate that negatively regulates insulin signaling. *Science* **332**, 1322–1326
- Entwisle, S. W., Martinez Calejman, C., Valente, A. S., Lawrence, R. T., Hung, C. M., Guertin, D. A., et al. (2020) Proteome and phosphoproteome analysis of brown adipocytes reveals that RICTOR loss dampens global insulin/AKT signaling. *Mol. Cell Proteomics* **19**, 1104–1119
- Yang, P., Humphrey, S. J., James, D. E., Yang, Y. H., and Jothi, R. (2016) Positive-unlabeled ensemble learning for kinase substrate prediction from dynamic phosphoproteomics data. *Bioinformatics* **32**, 252–259
- Zhao, Y., Xiong, X., Jia, L., and Sun, Y. (2012) Targeting Cullin-RING ligases by MLN4924 induces autophagy via modulating the HIF1-REDD1-TSC1-mTORC1-DEPTOR axis. *Cell Death Dis.* **3**, e386
- Casalou, C., Ferreira, A., and Barral, D. C. (2020) The role of ARF family proteins and their regulators and effectors in cancer progression: a therapeutic perspective. *Front. Cell Dev. Biol.* **8**, 217
- Donaldson, J. G., and Jackson, C. L. (2011) ARF family G proteins and their regulators: roles in membrane transport, development and disease. *Nat. Rev. Mol. Cell Biol.* **12**, 362–375
- Goldberg, J. (1998) Structural basis for activation of ARF GTPase: mechanisms of guanine nucleotide exchange and GTP-myristoyl switching. *Cell* **95**, 237–248
- Antonny, B., Beraud-Dufour, S., Chardin, P., and Chabre, M. (1997) N-terminal hydrophobic residues of the G-protein ADP-ribosylation factor-1 insert into membrane phospholipids upon GDP to GTP exchange. *Biochemistry* **36**, 4675–4684
- Cohen, L. A., Honda, A., Varnai, P., Brown, F. D., Balla, T., and Donaldson, J. G. (2007) Active Arf6 recruits ARNO/cytohesin GEFs to the PM by binding their PH domains. *Mol. Biol. Cell* **18**, 2244–2253
- Rosner, M., and Hengstschlager, M. (2007) Cytoplasmic/nuclear localization of tuberin in different cell lines. *Amino Acids* **33**, 575–579
- Schonbrun, M., Kolesnikov, M., Kupiec, M., and Weisman, R. (2013) TORC2 is required to maintain genome stability during S phase in fission yeast. *J. Biol. Chem.* **288**, 19649–19660
- Manning, B. D., Tee, A. R., Logsdon, M. N., Blenis, J., and Cantley, L. C. (2002) Identification of the tuberous sclerosis complex-2 tumor suppressor gene product tuberin as a target of the phosphoinositide 3-kinase/akt pathway. *Mol. Cell* **10**, 151–162
- Vander Haar, E., Lee, S. I., Bandhakavi, S., Griffin, T. J., and Kim, D. H. (2007) Insulin signalling to mTOR mediated by the Akt/PKB substrate PRAS40. *Nat. Cell Biol.* **9**, 316–323

44. Sancak, Y., Thoreen, C. C., Peterson, T. R., Lindquist, R. A., Kang, S. A., Spooner, E., *et al.* (2007) PRAS40 is an insulin-regulated inhibitor of the mTORC1 protein kinase. *Mol. Cell* **25**, 903–915
45. Wallroth, A., Koch, P. A., Marat, A. L., Krause, E., and Haucke, V. (2019) Protein kinase N controls a lysosomal lipid switch to facilitate nutrient signalling via mTORC1. *Nat. Cell Biol.* **21**, 1093–1101
46. Pan, C., Olsen, J. V., Daub, H., and Mann, M. (2009) Global effects of kinase inhibitors on signaling networks revealed by quantitative phosphoproteomics. *Mol. Cell Proteomics* **8**, 2796–2808
47. Murray, J. T., Campbell, D. G., Peggie, M., Mora, A., and Cohen, P. (2004) Identification of filamin C as a new physiological substrate of PKBalpha using KESTREL. *Biochem. J.* **384**, 489–494
48. Yoon, S. O., Shin, S., Liu, Y., Ballif, B. A., Woo, M. S., Gygi, S. P., *et al.* (2008) Ran-binding protein 3 phosphorylation links the Ras and PI3-kinase pathways to nucleocytoplasmic transport. *Mol. Cell* **29**, 362–375
49. Ghosh, P., Wu, M., Zhang, H., and Sun, H. (2008) mTORC1 signaling requires proteasomal function and the involvement of CUL4-DDB1 ubiquitin E3 ligase. *Cell Cycle* **7**, 373–381
50. Nie, X., Zheng, J., Ricupero, C. L., He, L., Jiao, K., and Mao, J. J. (2018) mTOR acts as a pivotal signaling hub for neural crest cells during craniofacial development. *PLoS Genet.* **14**, e1007491
51. Alvarado, E., Yousefalahiyeh, M., Alvarado, G., Shang, R., Whitman, T., Martinez, A., *et al.* (2016) Wdr68 mediates dorsal and ventral patterning events for craniofacial development. *PLoS One* **11**, e0166984
52. Boulay, P. L., Cotton, M., Melancon, P., and Claing, A. (2008) ADP-ribosylation factor 1 controls the activation of the phosphatidylinositol 3-kinase pathway to regulate epidermal growth factor-dependent growth and migration of breast cancer cells. *J. Biol. Chem.* **283**, 36425–36434
53. He, L., Gao, L., Shay, C., Lang, L., Lv, F., and Teng, Y. (2019) Histone deacetylase inhibitors suppress aggressiveness of head and neck squamous cell carcinoma via histone acetylation-independent blockade of the EGFR-Arf1 axis. *J. Exp. Clin. Cancer Res.* **38**, 84
54. Shome, K., Vasudevan, C., and Romero, G. (1997) ARF proteins mediate insulin-dependent activation of phospholipase D. *Curr. Biol.* **7**, 387–396
55. Haines, E., Schlienger, S., and Claing, A. (2015) The small GTPase ADP-Ribosylation Factor 1 mediates the sensitivity of triple negative breast cancer cells to EGFR tyrosine kinase inhibitors. *Cancer Biol. Ther.* **16**, 1535–1547
56. Karnam, P., Standaert, M. L., Galloway, L., and Farese, R. V. (1997) Activation and translocation of Rho (and ADP ribosylation factor) by insulin in rat adipocytes. Apparent involvement of phosphatidylinositol 3-kinase. *J. Biol. Chem.* **272**, 6136–6140
57. Kim, S., Heo, S., Brzostowski, J., and Kang, D. (2021) Endosomal mTORC2 is required for phosphoinositide-dependent AKT activation in platelet-derived growth factor-stimulated glioma cells. *Cancers (Basel)* **13**, 2405
58. Roux, K. J., Kim, D. I., Burke, B., and May, D. G. (2018) BioID: a screen for protein-protein interactions. *Curr. Protoc. Protein Sci.* **91**, 19 23 11–19 23 15
59. Eng, J. K., Jahan, T. A., and Hoopmann, M. R. (2013) Comet: an open-source MS/MS sequence database search tool. *Proteomics* **13**, 22–24
60. Elias, J. E., and Gygi, S. P. (2007) Target-decoy search strategy for increased confidence in large-scale protein identifications by mass spectrometry. *Nat. Met.* **4**, 207–214
61. Valot, B., Langella, O., Nano, E., and Zivy, M. (2011) MassChroQ: a versatile tool for mass spectrometry quantification. *Proteomics* **11**, 3572–3577
62. Schwanhauser, B., Busse, D., Li, N., Dittmar, G., Schuchhardt, J., Wolf, J., *et al.* (2013) Corrigendum: global quantification of mammalian gene expression control. *Nature* **495**, 126–127
63. Kim, D. H., Sarbassov, D. D., Ali, S. M., King, J. E., Latek, R. R., Erdjument-Bromage, H., *et al.* (2002) mTOR interacts with raptor to form a nutrient-sensitive complex that signals to the cell growth machinery. *Cell* **110**, 163–175
64. Rosner, M., and Hengstschlager, M. (2012) Detection of cytoplasmic and nuclear functions of mTOR by fractionation. *Met. Mol. Biol.* **821**, 105–124
65. Frias, M. A., Thoreen, C. C., Jaffe, J. D., Schroder, W., Sculley, T., Carr, S. A., *et al.* (2006) mSin1 is necessary for Akt/PKB phosphorylation, and its isoforms define three distinct mTORC2s. *Curr. Biol.* **16**, 1865–1870
66. Jain, A., Arauz, E., Aggarwal, V., Ikon, N., Chen, J., and Ha, T. (2014) Stoichiometry and assembly of mTOR complexes revealed by single-molecule pulldown. *Proc. Natl. Acad. Sci. U. S. A.* **111**, 17833–17838
67. Furman, C., Short, S. M., Subramanian, R. R., Zetter, B. R., and Roberts, T. M. (2002) DEF-1/ASAP1 is a GTPase-activating protein (GAP) for ARF1 that enhances cell motility through a GAP-dependent mechanism. *J. Biol. Chem.* **277**, 7962–7969
68. Horn, M., Geisen, C., Cermak, L., Becker, B., Nakamura, S., Klein, C., *et al.* (2014) DRE-1/FBXO11-dependent degradation of BLMP-1/BLIMP-1 governs *C. elegans* developmental timing and maturation. *Dev. Cell* **28**, 697–710
69. Gong, L., and Yeh, E. T. (1999) Identification of the activating and conjugating enzymes of the NEDD8 conjugation pathway. *J. Biol. Chem.* **274**, 12036–12042
70. Sanjana, N. E., Shalem, O., and Zhang, F. (2014) Improved vectors and genome-wide libraries for CRISPR screening. *Nat. Met.* **11**, 783–784
71. Cong, L., Ran, F. A., Cox, D., Lin, S., Barretto, R., Habib, N., *et al.* (2013) Multiplex genome engineering using CRISPR/Cas systems. *Science* **339**, 819–823